European **J**ournal of **Chem**istry

Check for updates

Band edge positions as a key parameter to a systematic design of heterogeneous photocatalyst

Eshraq Ahmed Abdullah

Department of Chemistry, Faculty of Education, Taiz University, Taiz, 009674, Yemen
ali123456yemen@gmail.com (E.A.A.)

* *Corresponding author at: Department of Chemistry, Faculty of Education, Taiz University, Taiz, 009674, Yemen.*
 Tel: +967.770120594 Fax: +967.4257802 e-mail: ali123456yemen@gmail.com (E.A. Abdullah).

REVIEW ARTICLE

KEYWORDS

ABSTRACT

Although, plenty of photocatalytic approaches have been developed in the past few decades to overcome major drawbacks, such as; wide band gap and fast volume/surface recombination of the charge carriers, the researchers still need to carry out careful systematic studies before conducting experiments based on physicochemical properties of a system. Thus, in this review, a detailed discussion of the band edge positions controlling the migration and charge separation of the produced charged carriers and its impact onto the photocatalytic systems are provided. The knowledge of band edge positions is a crucial prerequisite to a rational design of an efficient photocatalytic system. The enhancement mechanism should match these criteria to be reliable in the field of heterogeneous photocatalysis science.

1. Introduction

In the ultramodern era of technology, semiconductor photocatalyst still has been ranked as the most promising solutions for the energy crisis and environmental pollution due to its unique electronic band structure that absorbs the photons and creates active charge carriers for photochemical reactions. However, the limited numbers of visible light response semiconductor and the high recombination rate of the produced charge carriers limited the application of these materials. Thus, over the past decades, numerous promising approaches to develop visible light driven photocatalysts, including; metal/nonmetal doping [1-3] metal decorated [4], coupling with other semiconductor [5], Z-scheme hetero-structures [6] have been developed.

Recently, the ability of surface plasmon phenomena to harness a solar energy light showed a great interest of novel metal nanoparticles/semiconductor composite [7]. In addition, the short transportation length of charge carrier from the crystal interface to the surface and higher surface area to volume ratio when the scale confinement approaches to the Bohr radius create an attractive class of quantum dots (QDs) semiconductor candidates as luminescence probe for sensing events [8,9]. However, the blue shift of the band gap energy

hinders their visible light response. Therefore, band gap tuning by core/shell [10] and doped QDs [11] have been introduced as a promising class in solar photocatalyst design by many researchers.

These approaches were built based on band gap reduction in order to broaden the spectral response range of light and/or shifting the conduction band edge toward the negative potential and the valence band edge toward the positive potential which produce a thermodynamic favorable separation system of charge carriers [12]. However, it is difficult to realize the enhancement mechanism without systematic studies of physicochemical properties; band edge positions, band gap energy and charge carriers mobility prior to the fabrication process. Therefore, this review is an attempt to seek around physicochemical properties of all suggested approaches to gain understanding of how the produced charge carriers can be migrated and how the efficiency of the constructed photocatalyst will be enhanced. We hope this work will be used as a magic tool of the researchers to fabricate a new photocatalyst based semiconductor.

2. Semiconductor photocatalyst

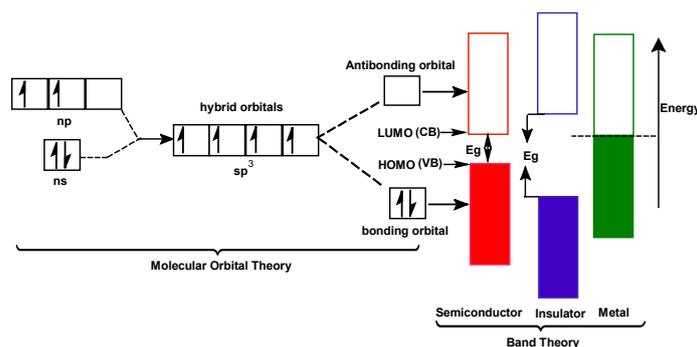A physical approach, Band Theory, categorizes solids
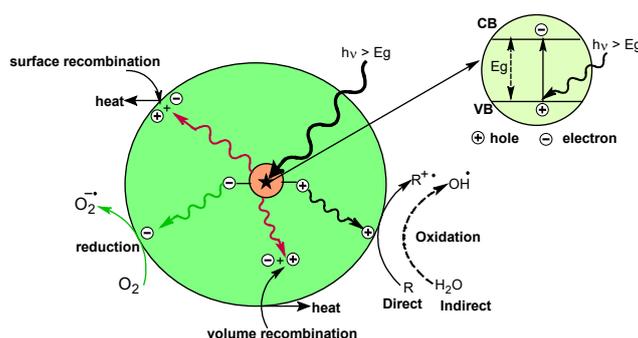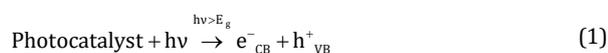
Figure 1. The structure of solids.

Figure 2. Photocatalytic mechanism [18].

according to forbidden region, which extends from the top of the filled valence band to bottom of the vacant conduction band into three categories. These categories are metal, semiconductor and insulator as shown in Figure 1 [13]. Chemically, the semiconductor solids construct by adding an enormous number of atoms using the building-up principle. When a second atom is brought up it overlaps with a first atom who contributes an orbital at a certain energy. The bonding (occupied) and antibonding (unoccupied) molecular orbitals only occur when the resulting system is energetically more favorable than unbound states [14,15]. The energy region between the highest occupied molecular orbital (HOMO), valence band (VB), and the lowest unoccupied molecular orbital (LUMO), conduction band (CB), is called the band gap (E_g).

The ability of any semiconductor to undergo sponta-neously photocatalytic reaction on its surface is governed by the relevant redox potential of the acceptor chemical species, which requires to be below (more positive) than the potential of the conduction band electrons, and the donor chemical species that needs to be above (more negative) than the potential of the valence band holes [16,17]. Beside the band edge positions the appropriate band gap energies of general catalytic reaction; water splitting and photodegradation of organic pollutants, are a convenient way to discover photo-catalytic semiconductor candidates. The choosing strategy is derived according to photocatalytic mechanism shown in Figure 2.

Once a semiconductor is exposed to an irradiation with an energy that overcomes the atomic band gap, an electron jumps from the valence band to the conduction band leaves behind a positively charged hole in the valence band. This mechanism can be simplified by Equation (1) [19].

$$\text{Photocatalyst} + h\nu \xrightarrow{h\nu > E_g} e^-_{CB} + h^+_{VB} \tag{1}$$

The target band gap should provide a sufficient nanosecond lifetime for the produced electron-hole pair to undergo charge transfer to the adsorbed molecule on the semiconductor surface. The charge and discharge on the semiconductor surface described by electron microscopy showed competition behaviour between a recombination process and the charge transfer of the produced electron-hole pair [20].

2.1. Recombination process

The accumulation of the electrons in the conduction band may encourage the recombination between negatively charged electron and positively charged hole. This may occur in the bulk (volume) of the semiconductor or via trapped at the surface with the release of heat,

$$e^-_{CB} + h^+_{VB} \rightarrow \text{Heat} \tag{2}$$

Thus, it is essential to measure the efficiency of the photocatalytic activity. However, due to the scattering process on the semiconductor surface, it is difficult to measure actual absorbed light. The quantum yield (QE%) of the photocatalytic reaction usually determines by the yield of a particular product as shown in Equation (3) [21].

$$QE\% = \frac{\text{Number of product formed for each electron}}{\text{Number of incident photons}} \times 100\% \tag{3}$$

2.2. Charge transfer from the valence band

Direct or indirect photo-hole reactions occurring at the edge position of the VB depend on its reduction potential with respect to the redox potential of the adsorbed molecule. The holes in the valence band should have a reduction potential in the range of +1.0 to +3.5 V versus the NHE. If the reduction potential of the adsorbed molecule is more negative than the

reduction potential of the VB holes, the produced holes undergo a direct photo-hole reaction [19,22].

$$h^+ + R \rightarrow R^{+\bullet} \rightarrow CO_2 + H_2O + \text{Degradation products} \quad (4)$$

Otherwise, the indirect hole reaction starts with the oxidation process of the adsorbed water or surface-bound hydroxide species. The edge position of the VB must be more positive than the potential needs to oxidize the water or hydroxide ion to hydroxyl radical (i.e. more positive than $E^0_{(H2O|OH^o)}$=2.38 V or $E^0_{(H2O|OH^o)}$=2.27 V *vs.* NHE) [23,24].

$$h^+ + \left(H_2O\right)_{ads} \rightarrow H^+ + OH^\bullet \quad (5)$$

$$h^+ + OH^- \rightarrow OH^\bullet \quad (6)$$

The produced hydroxyl free radicals disintegrate the harmful organic molecules and convert them into CO_2 and H_2O.

$$R + OH^\bullet \rightarrow R^{+\bullet} \rightarrow \rightarrow CO_2 + H_2O + \text{Degradation products} \quad (7)$$

In case of water splitting, the valence band edge potential should be below (more positive) the potential needs for oxygen evolution, i.e. $E_{O2/H2O}$= 1.23 V *vs.* NHE. However, the semiconductor band gap should not be wider in order to allow the absorption of visible light photons [25].

2.3. Charge transfer from the conduction band

The indirect degradation of organic molecule by using the conduction band electrons can only occur if the conduction band edge potential is more negative than the potential needs to reduce the adsorbed oxygen to superoxide. That is the conduction band edge potential must be more negative than -0.28 V vs. NHE [26].

$$O_{2ads} + e^- \rightarrow O_2^{\bullet-}{}_{ads} \quad E = -0.28 \text{ V} \quad (8)$$

In case of water splitting, the position of the conduction band edge should be above (more negative) the potential corresponding to the hydrogen evolution reaction [25].

A comprehensive analysis of the photocatalytic mechanism of the recently used semiconductors showed that a few number of normal semiconductor that match the electrode potential requirements is available to use. The bottom of the conduction band and the top of the valence band can be used as a good measure of the reduction and the oxidation power of photogenerated electrons and holes, respectively. The conduction band position of semiconductor photocatalyst should increase toward the vacuum level to ensure a high reducing capability of electrons. The valence band should rise to a narrower band gap and maintain the oxidation capability for holes. The value of the band gap of any semiconductor determines the range of wavelength that will be absorbed of the solar spectrum. The prediction of the band edge positions on the interface surface of an aqueous solution is an important task for photocatalyst design

3. Determination of the band edge positions

Band edge position of the conduction band (E_{CB}) can be derived experimentally from a flat band potential (E_{FB}) measurement, when the potential drop in the charge space layer is neglected, using various photo-electrochemical techniques, mainly; capacitance measurement. The flat band potential (E_{FB}) can be obtained from Mott-Schottky plot [27].

$$\frac{1}{C^2} = \frac{2}{\varepsilon\varepsilon_0 qN_D}\left(E_{appl} - E_{FB} - \frac{kT}{q}\right) \quad (9)$$

where C is the total capacitance of the two capacitors connected in series of the interface double layer capacitance (C_{SC}) and the Helmholtz layer capacitance (C_H), E_{appl} is the external applied potential, k is the Boltzmann constant, T is the temperature, q is the elementary charge, N_D is the doping density, ε and ε_0 are the relative permittivity of the semiconductor and vacuum, respectively. The flat band potential, the conduction band, of the pure anatase TiO_2 is -0.16 V versus NHE at pH = 0. Thus the position of the valence band edge can simply calculate through the Equation (10).

$$E_{VB} = E_{CB} + E_g \text{ ; where } E_{FB} = E_{CB} \quad (10)$$

Since the position of band edges in many cases cannot always be found in the literature or determine experimentally, the theoretical calculations provide a good tool to explore the band edge positions of the new fabricated materials from the Equation (11) [27-29].

$$E_{FB} = E^e - X + (1/2)E_g \quad (11)$$

Where X is the absolute electronegativity of the semiconductor, E^e is the energy of free electron on the hydrogen scale (4.44±0.02 eV) and the E_g is the band gap of the semiconductor. For example; the X value of TiO_2 equals to 5.8 eV and if we assume that the E_g = 3.2 eV yields the value of the band gap position of the TiO_2 conduction band of -0.24 V vs. NHE. This value is ~0.1 V more negative than the experimental value. However, not such simple deviation can always be occurred between the experimental and calculated determination, thus the combination of several methods is more reliable. Figure 3 depicts the band edge positions measured and/or calculated of several recently semi-conductors with the redox potential of hydrogen and oxygen evolution. However, based on the Nernst equation, each of these flat band potential values shifts 0.059 V to higher energy, more negative, for each pH unit increasing at 298 K [27].

$$E_{CB} = E_{FB} - 0.059 \times pH \quad (12)$$

In spite of the extensive efforts that have been done by the researchers, not all semiconductor band edge positions can match the electrode potential for superoxide production and/or direct/indirect holes oxidation. Also a few number of semiconductor materials are only suitable for hydrogen production, and some of them are good for oxygen production. Thus photocatalysis science stills a hot area of research up to date. An explanation of these efforts and the related mecha-nisms will be reviewed the following subsections.

4. Metal (cation) doping strategy

Metal doping is the process of adding foreign or impurity atoms in a crystal lattice of the semiconductor [43,44]. The difference between atomic radii of the metal (less than 15%), the similarity of the crystal structure and the electronegativity is the important criteria that should be matched to ensure meal doping solubility into the crystal lattice of the host photocatalyst, which is called a substitutional doping. Unless that the impurities will be presented between normal lattice sites, an interstitial doping. In addition, the metal doping choosing should exhibit different oxidation states. The possible trapping reactions of doping centers are described by the Equations (13 and 14).
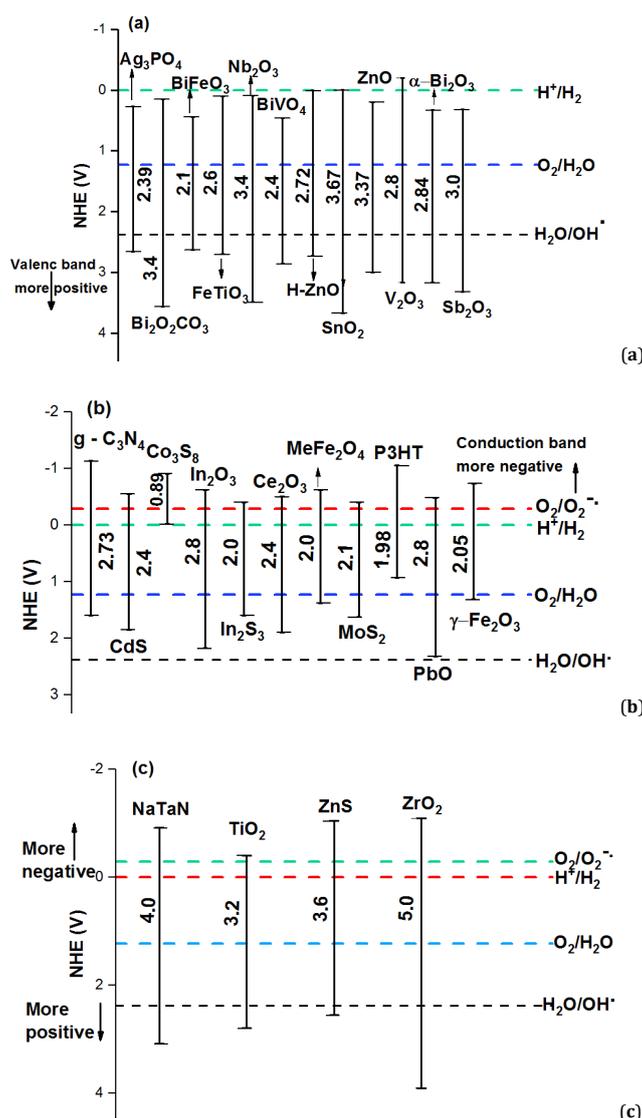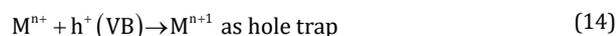
Figure 3. Band edge positions measured or estimated theoretically for several recently used semiconductors in aqueous media; (**a**) are the semiconductors where the valence band holes only match the potential needs for direct or indirect oxidation process, (**b**) are the semiconductors where the conduction band electrons only match the potential needs to reduce the adsorbed oxygen and (**c**) are the semiconductors where the produced charge carriers are powerful tools for oxidation and reduction processes [6,21,30-42].

$$M^{n+} + e^- (CB) \rightarrow M^{n-1} \text{ as electron trap} \tag{13}$$

$$M^{n+} + h^+ (VB) \rightarrow M^{n+1} \text{ as hole trap} \tag{14}$$

The electrode potential of $M^{n+}|M^{n-1}$ must be less negative than the reduction potential of the conduction band edge (lower), while the electrode potential of $M^{n+}|M^{n+1}$ must be less positive than the valence band edge (higher). The electron trapping level in the form of narrow band should be located slightly below the lower conduction band edge. That is the required energy level becomes

$$h\nu \geq E_g - E_t \tag{15}$$

where E_t is the lower edge of the trap level. Consequently, the recombination process is suppressed and the produced holes have enough time for a hydroxyl radical generation. However, a high concentration of metal dopants creates a new mid gap of surface states that promote electron-hole recombination

process [31]. The band gap narrowing mechanism using metal dopant strategy is shown in Figure 4.
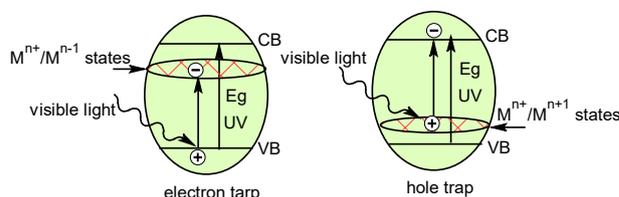

Figure 4. Metal doping strategy.

5. Metal-semiconductor strategy

The quantum yield of the photocatalytic activity was also enhanced by the addition of a metal which cannot be chemically bonded. This alternative modification process occurs on a semiconductor surface not in its crystal lattice [20].
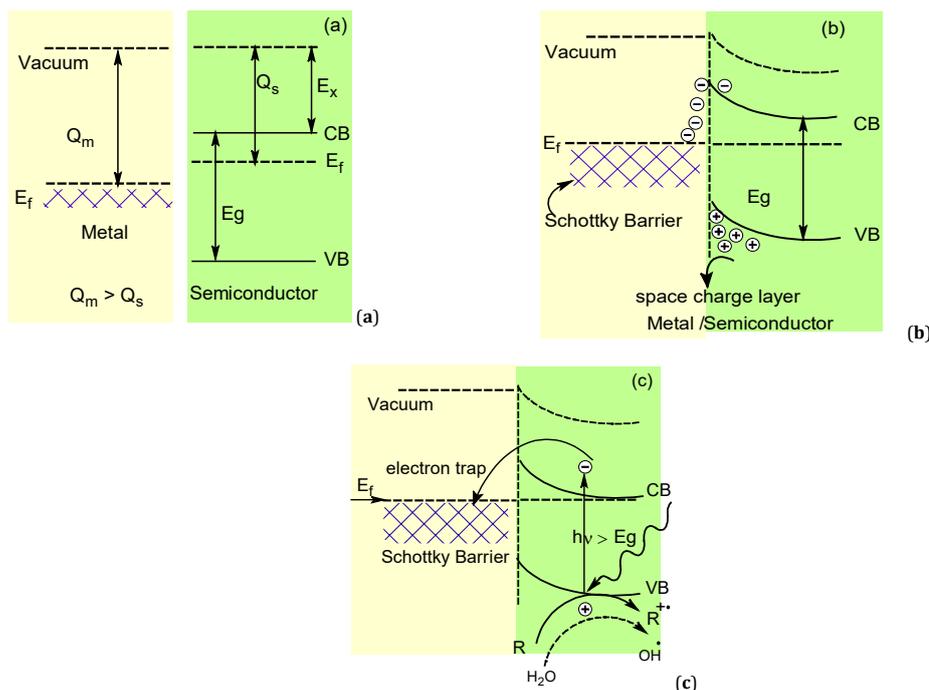
Figure 5. Metal-semiconductor strategy (**a**) before contact, (**b**) after contact and (**c**) after irradiation.

When the metal is deposited on the semiconductor surface, electrons will flow from the semiconductor conduction band to the metal until the two Fermi levels are aligned (equilibrated) [45]. This redistribution of the negatively charged electrons produces a space charge layer and develops an excess of positively charged holes in the valence band. A shift of an electrode potential of the conduction band will be occurring and the bands will be bent upward the semiconductor surface. The bending behaviour will therefore create a small barrier known as a Schottky barrier. The height of the Schottky barrier is given by Equation (16) [44].

$$Q_{Sch} = Q_m - E_x \qquad (16)$$

Where E_x is the semiconductor electron affinity, which is measured from the conduction band edge to the vacuum level of the semiconductor and Q_m is the work function of the metal, the minimum energy needs to remove an electron from the metal. This barrier serves as an electron trap providing better separation of charge carriers with a more oxidative power of semiconductor holes. The enhancement mechanism on Metal-semiconductor strategy is shown in Figure 5.

The previous analysis demonstrates that not all metals can be brought in contact with the semiconductor surface will enhance the photocatalytic activity. From a physics point of view, this only available if the work function of the deposited metal is bigger than the work function of the semiconductor, ($Q_m > Q_s$). That is, the reduction potential of the semiconductor conduction band must lie in a more negative than the Fermi level of the metal in the case of n – type semiconductor. In the p-type semiconductor, the oxidation potential of the valence band must be located in a more positive potential than the Fermi level of the metal [46].

6. Nonmetal (anion) doping

Nonmetal doping can broaden the visible light absorption region by raising the valence band edge significantly if the nonmetal has a comparable radius and lower electronegativity

compared to the nonmetal ions in the photocatalyst structure [47]. For example, nitrogen, carbon and fluorine have been cited in the literatures as an effective nonmetal doping of the semiconductor TiO_2 due to their comparably radius (r_N = 0.75, r_C = 0.77, r_F = 0.72) and lower electronegativity (EN_N = 3.0, EN_C = 2.5, EN_F = 4.0) compared to the oxygen atom (r_o = 0.73, EN_o = 3.5) who forms the TiO_2 valence band [48]. The large ionic radius of sulfur element r_s = 1.03 gives him the opportunity to occupy the lattice oxygen sites, anion doping, or titanium sties, cation doping. Although this conclusion opens a new insight of the researchers to choose any nonmetal doping to enhance the photocatalytic activity, the origin of the enhancement capacity remains unclear. Thus, several approaches have been used in the literatures to describe the origin of the visible light photocatalytic activity of nonmetal doped photocatalytic systems. For instant, Ran *et al.* proposed that nonmetal doping forms localized states within the band gap, mid gap state, via a mix of 2p electronic states of nonmetal with the 2p electronic states of the semiconductor which either interstitial or substitutions depending on synthesis conditions [38]. The energy level of these bands increases with decreasing the electronegativity of nonmetal dopant as shown in Figure 6. The ability of p-type doping to generate vacant states above the Fermi level with a red shift of optical absorbance edge, narrowing the band gap, was also confirmed by density functional theory calculation [49]. However, Nick Serpone argues the band gap narrowing and attributed the enhancement of TiO_2 photocatalytic activity in the visible light region to the formation of color centers [50]. This useful argument allows establishing a new co-doping semiconductor systems consisting of different combinations of metal and nonmetals. The presence of metal produces the Schottky trap level that has the capacity to promote charge separation, while the nonmetal ions creates the visible light absorption centers.

7. Surface sensitization

A wide band gap semiconductor can be sensitized by using chemisorbed or physisorbed chemical species.
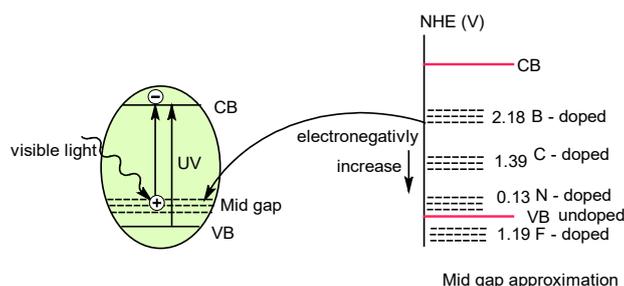
Figure 6. Mid gap approximation for non-metal doped. The mid gap positions of different non-metal anions have been taken from [47].
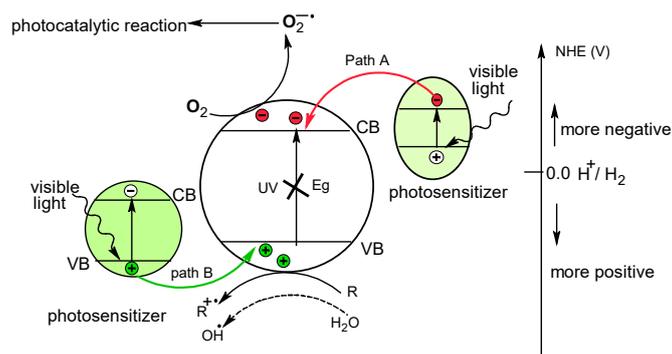

Figure 7. Surface sensitization electrode potential requirements.

The sensitization process only occurs if the reduction potential of the excited state either singlet or triplet of the sensitizer molecule with respect to the conduction band edge is more negative (high enough). The sensitizer molecule permits the transfer of the electron to the conduction band semiconductor. The photogenerated electron used to form superoxide $O_2^{-\cdot}$ and hydroxyl radicals, which are responsible for the photodegradation process. This process is shown in path A Figure 7 [51].

However, the photocatalyst may lose its response in the visible light region, when the photosensitizer molecule undergoes a rapid mineralization due to the presence of the oxygen/air interface. Thus, some researchers suggest the use of a narrow band gap Nano crystalline semiconductor such as; multi-walled carbon nanotube (MWCNT) or metal oxide like CuO and Cu_2O as a sensitizer for the visible light response [52]. According to relative band edge positions, another photo-sensitizer, holes sensitizer, can also be designed if the valence band of the sensitizer is located at a more positive potential than that of the semiconductor valence band edge. The holes can be transferred to the semiconductor valence band (through path B) and initiate direct or indirect oxidation reaction [53].

8. Synergetic effect of semiconductor -carbon composite

Different types of semiconductor-carbon heterostructure composite including; activated carbon, carbon nanotubes (CNTs), multi walled carbon nanotubes (MWCNT) and graphene have been designed in the literatures due their promising properties. For example; the large surface area of activated carbon enhances the adsorption ability of a pollutant which is the first step determining photocatalytic activity [54]. The metallic conductivity of CNTs and graphene forms a Schottky barrier that can be used as an electron trap center with a large storage capacity of photoexcited electrons [19]. As a result of these properties, three mechanisms have been cited in the literature to describe the synergistic effect of carbon on

the TiO_2 photocatalyst surface. The relative positions of the conduction band edge of TiO_2 (-0.3 V vs. NHE) and nanocylinder carbon (CNTs) of (+0.3 V vs. NHE) suggest that the CNTs act as an efficient electron sink that prevents the possible recombination with the produced hole in the semiconductor valence band [55]. A second mechanism explained by Dai *et al.* who attributed the synergistic effect of MWCNT on TiO_2 to a photosensitizer behavior, which pumps the electrons into the TiO_2 conduction band. Beside that, carbon can also easily act as a template to facilitate the dispersion of the TiO_2 particle and hinder the agglomeration [52]. The Synergistic effect of semiconductor-carbon composite of some systems is shown in Figure 8.

9. Coupled semiconductor composites

Another strategy to facilitate charge transfer and separation is to combine one semiconductor with another that has a suitable band gap [56]. Band structure design of coupled semiconductor depends on the relative edge positions of the conduction and valence bands for the two semiconductors. Assuming that the coupled semiconductor system consists of A and B materials, three types of how does the heterostructure construct, have been proposed in the literatures [57]. As shown in Figure 9, Type (I) forms when the conduction band edge position of the semiconductor A is higher than that of the semiconductor B, and the valence band edge position of A is lower than B. For lower energy, electrons and holes tend to move downward and upward, respectively, and get accumulated in the semiconductor B. In type (II), the conduction and valence band edge positions of the semiconductor A are both lower than those of the semiconductor B leading to a significant charge carrier separation. Type (III) has the same structure of type (II) with large differences on the edge band positions. The enhancement mechanism can be approached depending on the band edge positions of both semiconductors.
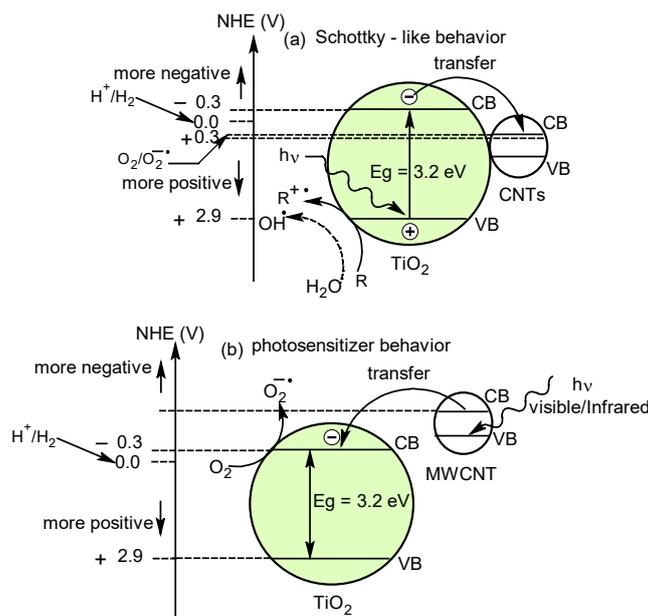
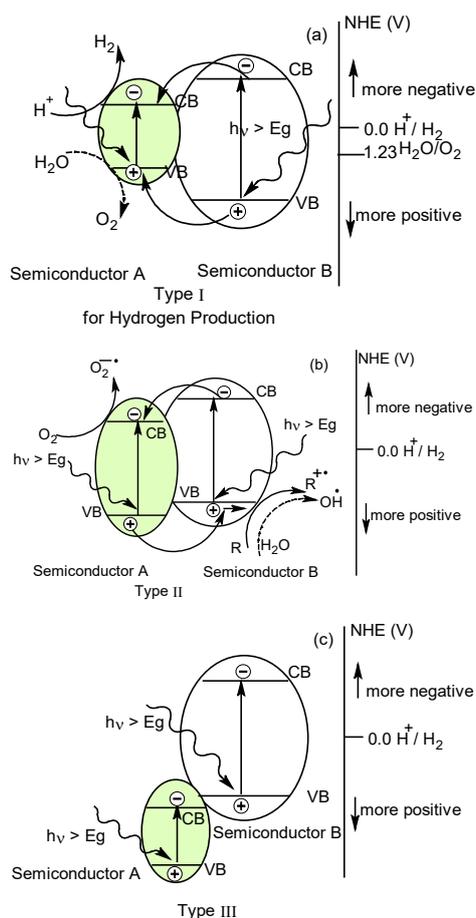**Figure 8.** The Synergetic effect of semiconductor-carbon composite.

Figure 9. Electrode potential of heterostructure semiconductor composites [57,58].

For example, in type (II) the conduction band of the semiconductor A is more positive than that of the semiconductor B, thus the electrons will flow to the semiconductor A conduction band under UV/visible light irradiation. Since the valence band edge position of the semiconductor A is more positive than that of the semiconductor B, the holes can transfer to the semiconductor B valence band producing a good charge separation mechanism [19].
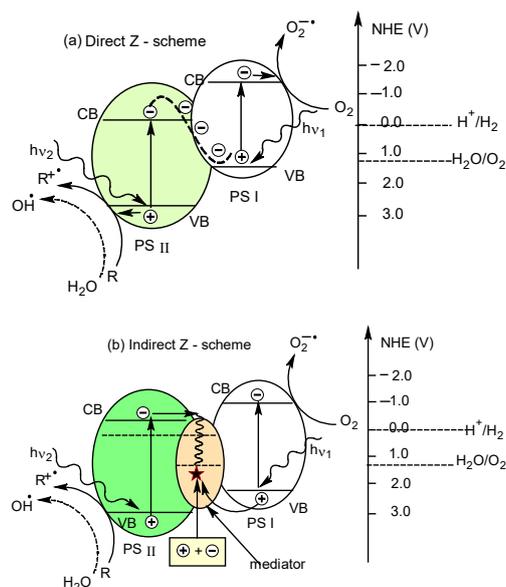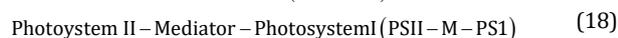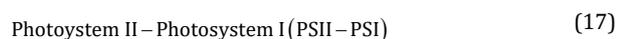
Figure 10. Z-Scheme photocatalytic mechanism.

10. Z-Scheme semiconductor composites

The construction of coupled semiconductors which usually belongs to the type II and a few of type I is considered as a good method to enhance the quantum yield of photocatalytic activity due to the efficient separation techniques of charge carriers. However, the resulted photo-excited electrons and holes still less active than a single component photocatalyst system. Therefore, a Z-scheme concept is suggested as a new promising strategy to devise the photocatalytic systems with greater efficiency. The Z-scheme photocatalyst can be defined as a system that has a charge transfer mechanism similar to that of the natural photosynthesis in green plants or the system whose its charge carrier transport looks like the English letter (Z) and consists of two step photo-excitation [59]. This system can be summarized by using Equations (17 and 18). The first one is for a direct Z-scheme photocatalyst while the second one is referred to an indirect Z-scheme photocatalyst system.

$$\text{Photoystem II} - \text{Photosystem I}\left(\text{PSII} - \text{PSI}\right) \qquad (17)$$

$$\text{Photoystem II} - \text{Mediator} - \text{PhotosystemI}\left(\text{PSII} - \text{M} - \text{PS1}\right) \qquad (18)$$

Although a direct Z-scheme system does not contain the mediator and its structure is similar to type II hetero-structure coupled semiconductors, the charge carrier transport mechanism and efficiency are totally different. The mediator system of the indirect Z-scheme systems can be liquid phase acceptor/donor chemical species or a conductive medium such as a noble metal in solid state systems [60]. The electrode potential requirements of the construction of the Z-scheme can be generalized into three points; firstly, a suitable band alignment to ensure a strong oxidation ability of the photo-generated holes in the valence band of PSII which can be maintained if the PSII valence band potential is more positive than those of the redox potential of adsorbed water or organic pollutants. And the PSI conduction band edge potential should be more negative compared to that of the PSII and the redox potential of a superoxide radical to exhibit a strong reducing ability of excited electrons. Secondly, short distance between the valence band of PSI and the conduction band of PSII. Finally, the formation of contact interface or ohmic contact,

thus, the electrons in the conduction band of PSII and the holes in the valence band are annihilated via a direct contact or the mediator, providing a great separation efficiency and high redox ability [61]. The Z-scheme photocatalytic mechanism is shown in Figure 10.

11. Plasmonic metal nanoparticles-semiconductor composite

Beside the synergistic effect of a Schottky junction center trap at the metal/semiconductor interface, the Combination of the novel metals catalytic activity with a light absorption ability of a nanoscale dimension presents a chance to seek the probability to design a new class of visible light driven photocatalyst based on noble metal nanoparticles–wide band gap semiconductor composite which is called NPs plasmonic photocatalyst [62]. However, the high cost of noble metals inhibits the ability of large scale applications and opens a way of non-element metal such as; metal oxide/sulfide to be a potential substitute for plasmonic noble metals [63]. A good choice of the plasmonic nanostructure and the ability to design an effective interface between plasmonic and semiconductor requires a full understanding of plasmonic resonance mechanism/definition.

11.1. Plasmonic resonance mechanism/definition

When the novel metal nanoparticles or plasmonic nanostructured materials are irradiated with electromagnetic energy in the visible or infrared regions, trapped photons polarize the free conduction electrons to one side of the novel metal surface. As a result, a restoring force arising from the positive nuclei redistributes the surface charge and creates an electric field [64]. The produced local electric field causes collective oscillations of the conduction electrons at the interface between a nanoparticle and semiconductor. If the incident light has a frequency around the frequency of oscillated surface electrons, the resonance is occurring, which is called localized surface plasmon resonance (LSPR), and the free electrons of NPs gain the light energy (become plasmonic particles). The high–energy resonant states can return to their ground states in three possible forms; release the energy as a heat to the lattice and the surrounding media, radioactive
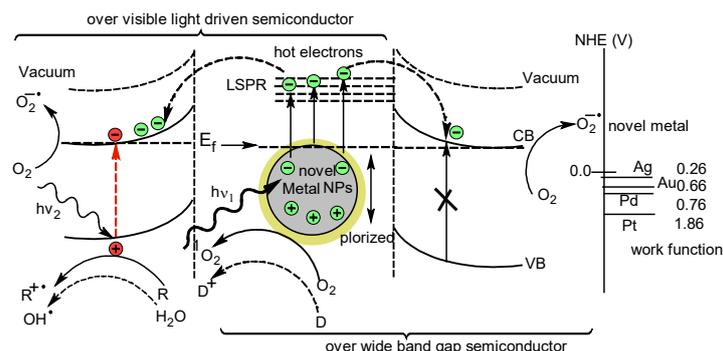
Figure 11. The Major processes in the plasmonic photocatalysis, the values of novel metals' work functions were calculated from the reference [16].
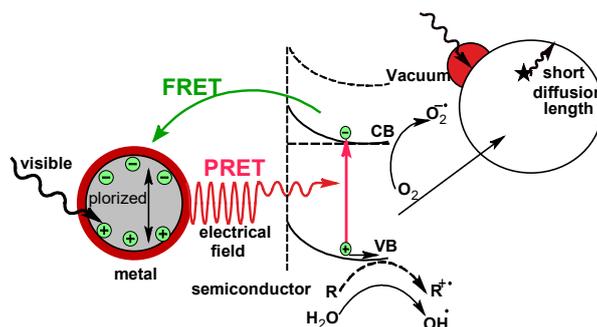

Figure 12. Schematic diagram of PRET excitation mechanism.

re-emission (scattering) of photons and the generation of energetic electrons which are not in thermal equilibrium, hot electron [45]. However, the ability of LSPR excitation of visible light to generate the hot electrons depends on the size and shape of the nanoparticles. The hot electrons can be injected into a semiconductor in direct contact with a nanoparticle metal, which is called plasmonic metal/semiconductor hybrid. That is the metal works as a sensitizer to supply the electrons to the semiconductor conduction band. However, there is great debate among the researchers about how the electrons are transferred under light irradiation in the presence of a Schottky barrier. Actually, the benefits of the LSPR pheno-menon into the design of visible light photocatalysts only occur if the hot electrons gain sufficient energy (E_{LSPR} (eV)) to overcome the Schottky barrier (E_{SB} (eV)) produced at the metal-semiconductor interface, (i.e., $E_{LSPR} > E_{SB}$). In general, the interband transitions rate increases if the energy level of the generated hot electrons by LSPR ($E_f + h\nu$) is more negative than that of the semiconductor conduction band edge. And the conduction band edge of the wide gap semiconductor must be moderate (not too negative in potential) to ensure well-established of the space charge layer with a suitable thickness for electron injection along the bent conduction band [45,46]. On the basis of stability point of view, the remaining hot holes left in the metal NPs should be compensated by using an electron donor or a hole-transporting material in order to retain a sustainable LSPR. Nguyen and Nguyen suggested that this process can be done through a generation of singlet oxygen [65]. In case of visible light driven semiconductor the LSPR effect of the hybrid novel metal NPs/semiconductor depends on the wavelength of the incident light. For example the Au nanoparticles can enrich the g-C_3N_4 surface by the hot electrons together with photogenerated electrons in the g-C_3N_4 conduction band only in the wavelength range of 460 > λ < 640 nm, while in the range of 400 < λ < 460 nm, Au works as an electron trap through the formation of a Schottky barrier [66]. The major processes in the plasmonic photocatalytic mechanism are shown in Figure 11.

The existence of an intense oscillating electric field around the metal suggests another mechanism that can be used to enhance the photocatalytic activity called Plasmon Resonance Energy Transfer (PRET). According to the PRET approach, the energy can transfer from the Plasmon NPs metal to the semiconductor surface via the electrical field. This electrical field able to promote the rate of electron-hole formation at well-defined locations, called hot spots, and cause an increase in the power absorption in this region. The generated hot spots are confined to a few nanometers of the semiconductor surface, thus the diffusion length becomes shorter without undergoing recombination compared to non-plasmonic semiconductor as shown in Figure 12 [67]. Unlike hot electron approach, the PRET is not limited by the Fermi level equilibration between the metal and the semiconductor. Thus the ultimate contact is not essential. However, the main points in the PRET technique are the presence of the semiconductor within the range of the produced field and a spectral overlap occurring between the LSPR excitation and the semiconductor absorption [68].

12. Quantum confinement and a core/shell semiconductor photocatalyst

To understand the transformation occurring on the photocatalyst surface at a molecular level, the relationship between band gap change and a particle size has been reviewed in many literatures [69]. As the size of the particle decreases, the specific surface area of a catalyst increases. When the particle diameter is reduced to a few 10s of nanometer, the surface atomic structure starts to lose its stoichiometry due to the reduction of neighbor atoms and lower binding energy per atom in the crystal lattice [70]. As a result, the density of surface defects, excess oxygen atoms, of metal oxide semiconductor crystalline increases and creates deep and shallow traps near the band edge.
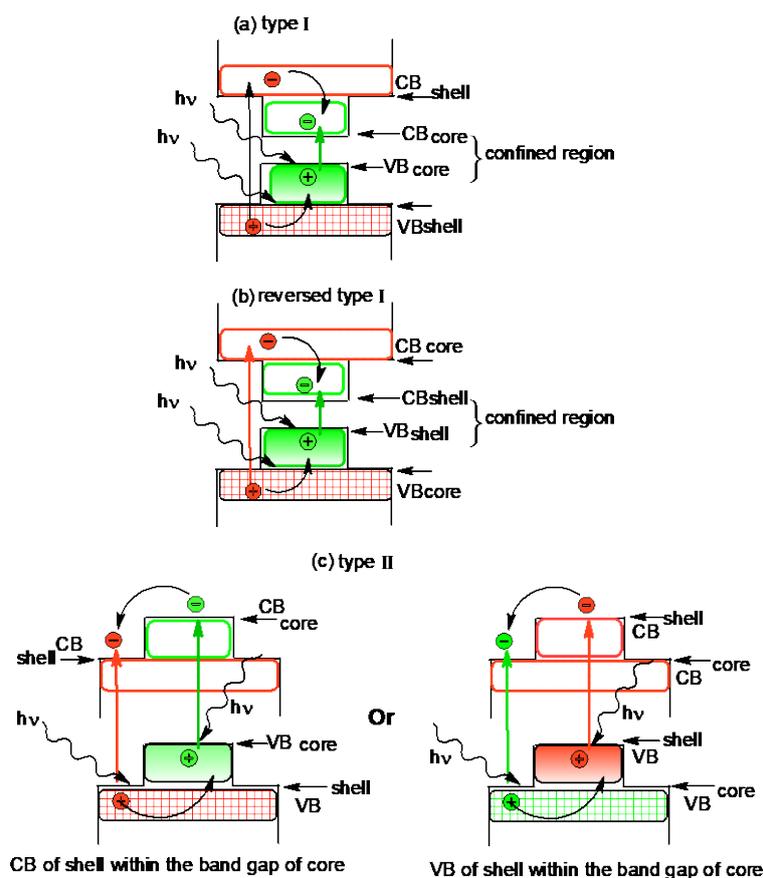
Figure 13. Schematic representation of the energy-level alignment in different core/shell systems.

Thus the band gap is reduced, red-shift in absorption spectrum, without shifts of the edge positions of the conduction and valence band (that is the photocatalyst semiconductor's color stills the same) and the diffusion of the charge carriers is enhanced and the probability of electron-hole recombination is decreased [71]. Continuing decreasing the particle size to near its Bohr radius, a quantum confi-nement takes place due to a drastic change in the electronic properties of the particle. Quantum confinement can be defined as the widening of the band gap energy of the semiconductor when its size has fallen below the critical radius, below 10 nm. In this case, the photo-excited electron hole pair behaves like a hydrogen atom where the hole forms a nucleus resulting in a spatial confinement of charge carriers. The distance between the electron and hole is defined as the exciton Bohr radius [72]. That is the confinement effect becomes prominent only if the dimension of the semicon-ductor crystal equals or less than the exciton diameter. If the excitons of the solid are confined into two-dimensional sheet of the order of the Bohr radius, the exctions need to treat as particles in a quantum well. This type of structure is also known as a 2D nanostructure or nanosheet because of the excitons motion is restricted along a 2D plane [9]. The band edge alignments and mechanisms of quantum well confined systems are not different than that of bulk or nanostructures heterostructure systems discussed before.

12.1. Core/shell or sandwiched semiconductors

Among different confined systems, core/shell or sandwiched semiconductors are still an interested class of recent developed photocatalysts compared to simple hetero-structure systems. In general, the appropriate band edge positions classify core/shell systems into three types; type I, reversed type I and type II as shown in Figure 13. In type I, the valence band edge, and conduction band edge of the quantum well or the sheet (the core) completely falls between the valence band edge, and the conduction band edge of the second semiconductor (the shell). In such situation, both electrons and holes are confined into the core semiconductor. In the reversed type I, the band gap of the shell semiconductor is smaller than that of the core semiconductor, however, the holes and electrons may not completely confined in the shell due to shell thickness effect. In type II, either the valence-band edge or the conduction band edge of the shell semiconductor is located within the band gap of the core providing, a good spatial separation of the charge carriers in different regions of the core/shell structure [10].

These alignment types also can be appeared if the solid excitons able to move along one direction, which is called a 1D nanostructure or quantum wire. The structure consists of 2 nm cross-section long tube of the lower band gap semiconductor surrounded by the larger gap semiconductor. In a zero dimension (quantum dots) solid, the excitons are confined in all directions and the quantum dots are made by using lower band gap semiconductor surrounded by the higher band gap semiconductor [9]. According to the effective mass approximation theory, the band gap energy due the quantum size effect (E(R)) is expressed as

$$E(R) = E_g + \frac{h^2}{8\mu R^2} - 1.786 \frac{e^2}{\varepsilon R} - 0.248 \, E_{Ry} \qquad (19)$$

where E_g is the band gap of the bulk semiconductor, μ is the reduced effective mass, R is the radius of the spherical semiconductor, h is the Plank's constant, e is the charge of the

electron, ε is the dielectric constant and E_{Ry} is the Rydberg energy constant. The correlation between band edge positions and the confinement energy shows that the increase in the band gap energy of a semiconductor increases the lifetime of electrons and holes leading to drastically reducing of the recombination process. The ability of quantum dots to convert near infrared light to visible light, the high surface area to volume ratio and the shorter transportation length of the charge carriers enhance the quantum yield of the photocatalytic reaction and classify the quantum confined core/shell semiconductors as a promising way for many researchers in the recent years. However, the understanding of band edge alignments is not enough to fabricate a good core/shell photocatalyst system. The core/shell materials should be also crystalized in the same structure with a small lattice mismatch in order to prevent the trap states formation at core/shell interface or within [10].

12.2. Doping in quantum dots (QDs)

Semiconductor quantum dots are another attractive class of nanomaterials that have been receiving much attention as advanced photocatalytic materials, in recent years, due to the high value of extinction coefficient and enhanced quantum yield about three electrons per photon compared to bulk semiconductor. However, the high energy gap of QDs reduces the amount of photon being absorbed in the solar spectrum [12]. Therefore, Doped QDs have lately suggested as an important aspect for solar energy photocatalyst [73]. The presence of dopants perturbs the band structure by modifying the density of states within the band gap. The new created energy state below or above the conduction and the valence band edge, respectively, traps the charge carriers and drastically reduce the recombination rate as described in Figures 4 and 6. The potential used of QDs as fluorescent donors via Fluorescence (or Forster) resonance energy transfer (FRET), which involves a non-irradiative energy transfer between a donor who is in an excited electronic state to a nearby acceptor in the ground state through a long-range dipole-dipole interaction, has been explored [74,75]. This energy transfer is thermodynamic favorable as soon as the position of the conduction band edge can move up to more negative potential and the position of the valence band edge moves towards more positive potential as a result of the confinement effect [12]. The applications of doped QDs in FRET-based sensor have been cited in the literature [76], while the impact of the FRET mechanism in the photocatalytic activity of QDs has not been fully understood so far. However, the back transfer of excited carrier by the FRET mechanism which takes away the excited carriers from the semiconductor to plasmon metal shown in Figure 12 reduces the energy transfer via the PRET mechanism [77]. Thus, it is better to distinguish between the two processes to describe the photocatalytic enhancement mechanism.

13. Results and discussion

You may be surprised to see this section in a review paper; however, the idea was developed in order to attract the attention of the reader to the importance of the topic. Actually, this section is attempting to redraw some of the successfully built photocatalytic systems that have been cited in the literatures in order to seek the ability of band edge alignment approximation to describe the occurrence, enhancement of photocatalytic mechanism and the involved photochemical species. For example, a schematic diagram of the Yb^{3+}/Tm^{3+} co-doped In_2S_3 (YTIS) can be redrawing based on band edge alignment in the Figure 14 [2]. The presence of the intermediate energy states and/or sulfur vacancies below the conduction band provides an efficient separation rate and

hinders carrier recombination. The more negative conduction band edge of -0.41 V *vs*. NHE compared to redox potential of Cr(IV)/Cr(III) of 0.51 V *vs*. NHE facilitates the direct reduction process of conduction band electrons. The higher energy of LUMO level of RhB dye (around -1.0 V *vs*. NHE) than the YTIS conduction band edge is another path to promote the electron injection to YTIS conduction band by photosensitization effect. The produced electrons at the conduction band edge can also be used to form superoxide radicals that capable to reduce the RhB+. molecule. Unfortunately, the more positive edge of the valence band hole hinders the direct/indirect oxidation of RhB+. molecule. However, the production of oxygen at In_2S_3 valence band edge facilitates a rapid mineralization of RhB+. molecule at the semiconductor/electrolyte interface.
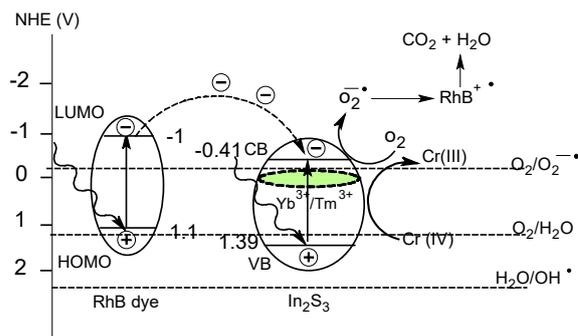
Figure 14. Schematic diagram of photocatalytic process of YTIS for Cr (VI) and RhB degradation [2].

The short distance between the valence band edge of conjugated polymer P3HT (-1.05 *vs*. NHE) and the conduction band edge of hierarchical ZnO (H-ZnO) supports the electron migration and annihilation with the P3HT valence band holes producing a direct Z-scheme heterostructure photocatalyst. Hence, the accumulated electrons on P3HT conduction band reduce the adsorbed O_2 to form O_2^- radicals, and the H-ZnO valence band holes become free to undergo a direct/indirect oxidation process with the adsorbed pollutant as shown in Figure 15 [6].

In contrast, long distance between the Ag_3PO_4 conduction band edge (0.27 V *vs*. NHE) and the $BiVO_4$ valence band edge (2.86 V *vs*. NHE) prevents a direct flow of the Ag_3PO_4 electrons. In addition, the accumulated electrons on the $BiVO_4$ conduction band edge cannot reduce the O_2 to form O_2^- and the migration of holes towards the Ag_3PO_4 valence band decreases their oxidation ability due to the more positive edge potential. Thus, Chen *et al.* constructed an indirect Z-scheme by using grapheme bridged and Ag metal [33]. On the basis of band edge approximation, the metal Ag acts as a cross linking bridge (mediator) for the two semiconductors.
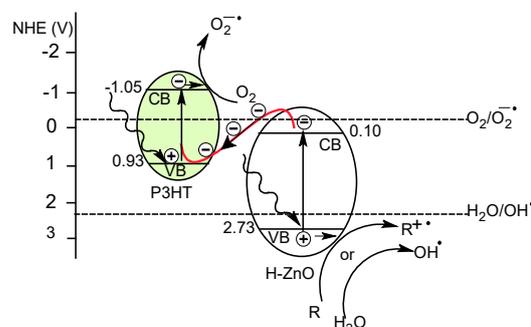
Figure 15. Schematic illustration of the charge carrier transport mechanism over P3HT/H-ZnO.

The $BiVO_4$ electrons and Ag_3PO_4 holes quickly transfer to Ag metal in order to achieve an efficient carrier separation. The more positive edge of the Ag_3PO_4 conduction band (0.27 V *vs.* NHE) prevent the superoxide formation which may decrease the photo-stability of the constructed system. Thus, the authors introduce a zero band gap material, graphene, as an electron sink that capture the Ag_3PO_4 conduction band electrons and enhance the photo-stability of the catalyst as described in Figure 16.

Figure 16. Schematic illustration of the charge carrier transport mechanism over graphene-bridged $Ag_3PO_4/Ag/BiVO_4$.

An example of a partially suitable design of type II hetero-structure has been shown for two-dimensional nanosheets $SbN_2O_6/g-C_3N_4$ by Zhang *et al.* [41]. The $g-C_3N_4$ conduction band electrons directly inject to the more positive SbN_2O_6 conduction band facilitating the production of a superoxide radical, while the holes slant to migrate to $g-C_3N_4$ valence band. However, the more negative edge of $g-C_3N_4$ limits their ability to produce a hydroxyl radical and may decrease the photo-stability of the system in the absence of hole scavenge materials as shown in Figure 17.
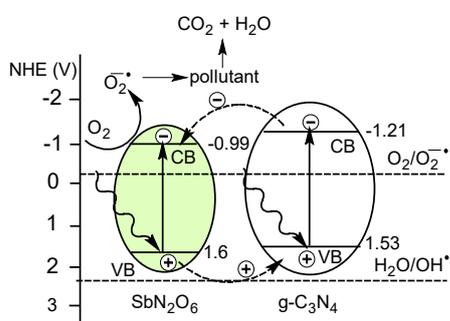

Figure 17. Schematic illustration of the charge carrier transport mechanism over SbN2O6/g-C3N4.

The band edge alignment approach can also be used to elucidate confusion in the enhancement mechanism over $Au/g-C_3N_4$ photosensitizer by Xie *et al.* [66]. Based on the metal/semiconductor strategy, the conduction band electrons should flow from the $g-C_3N_4$ semiconductor conduction band to the metal Au which acts as an electron sink due to the formation of a Schottky barrier at the metal/semiconductor interface. This will hinder the electron-hole recombination by prolonging the lifespan of the electrons. However, the accumulated electrons at a Schottky edge are unable to produce the hydrogen due its more positive potential than the redox potential of water ($E_{H2O/H2}$ = -0.8227 *vs.* NHE). Thus the authors introduce the idea of the hot electrons injection through SPR mechanism to explain the enhanced rate of hydrogen production as shown in Figure 18. The PRET is another mechanism that can also be taken into account to explain the photocatalytic activity of the $Au/g-C_3N_4$ system, where the generated carriers can diffuse safely to the surface without undergoing recombination.
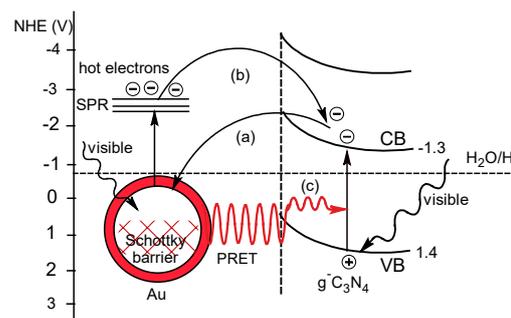

Figure 18. Schematic illustration of the charge carrier transport mechanism over $Au/g-C_3N_4$, (a) is a Schottky trap mechanism, (b) is a hot electron approach and (c) is a PRET approach.

While Chen *et al.* used this approach, to predict the type of active chemical species responsible of photocatalytic activity of carbon quantum dots modified BiOI microsphere [78]. The small band gap of 1.8 eV makes BiOI easily to excite by visible light, however, the more positive edge of the BiOI conduction band (0.6 V *vs.* NHE) suppress the production of a superoxide radical. Hence, a hydroxyl radical could only be produced by indirect holes oxidation of water or hydroxyl ion as described by Equations (5) and (6).

14. Conclusion

As noted throughout the text, the practical utilization of any photocatalyst system needs to be approached in a different way, i.e. based on its physicochemical properties mainly; band edge positions, band gap energy and charge carrier mobility. Also the suggested mechanism of the const-ructed photocatalyst must be corresponded with these physicochemical standards to be precision. The band edge positions in many new developed materials cannot be simply taken from the literatures which make a big confuse of the researcher when he try to explain the enhancement mechanism. The combination between the experimental and the theoretical calculations will give more confident results and enhance our understanding of the photocatalytic mechanism of the developed materials. Although a great progress has been achieved in this area of research, the development of some approaches, such as; Z-scheme, plasmonic NPs semiconductor, confined core/shell semicon-ductors and doped QDs still in the early stage and facing a lot of challenges that should be addressed. The potential application of plasmonic NPs semiconductor in the photo thermal treatment of cancer encourages the researchers to build a new system that can use visible light instead of harmful radioactive materials that damage the normal tissue of cells. Additionally, understanding the photocatalytic mechanism is a helpful way to enhance the stability, reuse-ability of photo-catalytic systems which still a challenge area in photocatalysis fabrication.

Disclosure statement DS

Conflict of interests: The author does not have any conflicts of interest
Ethical approval: All ethical guidelines have been adhered

ORCID iD

Eshraq Ahmed Abdullah
iD http://orcid.org/0000-0001-9698-6203

References

[1]. Guo, S.; Deng, Z.; Li, M.; Jiang, B.; Tian, C.; Pan, Q.; Fu, H. *Angew. Chem.* **2016**, *128*, 1862-1866.
[2]. Wu, Z.; Yuan, X.; Zeng, G.; Jiang, L.; Zhong, H.; Xie, Y.; Wang, H.; Chen, X.; Wang, H. *Appl. Catal. B: Environ.* **2018**, *225*, 8-21.
[3]. Zhang, X.; Qin, J.; R.; Hao, Wang, L.; Shen, X.; Yu, R.; Limpanart, S.; Ma, M.; Liu, R. *J. Phys. Chem. C* **2015**, *119*, 20544-20554.
[4]. Lee, J.; Shim, H. S.; Lee, M.; Song, J. K.; Lee, D. *J. Phys. Chem. Lett.* **2011**, *2*, 2840-2845.
[5]. Siuleiman, S.; Kaneva, N.; Bojinova, A.; Dimitrov, D.; Papazova, K. *Bulg. Chem. Commun.* **2017**, *49*, 199-204.
[6]. Liu, H.; Li, M.; Yang, J.; Hu, C.; Shang, J.; Zhai, H. *Mater. Res. Bull.* **2018**, *106*, 19-27.
[7]. Lou, Z. Z.; Kim, S.; Fujitsuka, M.; Yang, X.; Li, B. *Adv. Funct. Mater.* **2018**, *28*, 1706969.
[8]. Wang, J.; Tang, L.; Zeng, G.; Deng, Y.; Dong, H.; Liu, Y.; Wang, L.; Peng, B.; Zhang, C.; Chen, F. *Appl. Cata. B-Environ.* **2018**, *222*, 115-123.
[9]. Rajabi, H. R. Photocatalytic Activity of Quantum Dots, in: Semiconductor Photocatalysis-Materials, Mechanisms and Applications, InTechopen, 2016.
[10]. Reiss, P.; Protiere, M.; Li, L. *Small* **2009**, *5*, 154-168.
[11]. Shamsipur, M.; Rajabi, H. R.; Khani, O. *Mater. Sci. Semicond. Process.* **2013**, *16*, 1154-1161.
[12]. Kandi, D.; Martha, S.; Parida, K. *Int. J. Hydrogen Energy* **2017**, *42*, 9467-9481.
[13]. Lazar, M.; Varghese, S.; Nair, S. *Catalysts* **2012**, *2*, 572-601.
[14]. Atkins, P.; De Paula, J. Atkins' Physical Chemistry, 9th Edition, Oxford University Press, 2009.
[15]. Ren, X. F.; Zhang, J.; Kang, G. J. *J. Nanomater.* **2015**, *2015*, Article ID 605728, 9 pages.
[16]. Zhang, X.; Chen, Y. L.; Liu, R. -S.; Tsai, D. P. *Rep. Prog. Phys.* **2013**, *76*, 046401.
[17]. Makama, A. B.; Umar, M.; Saidu, S. A. CQD-Based Composites as Visible-Light Active Photocatalysts for Purification of Water, InTechopen, 2018.
[18]. Linsebigler, A. L.; Lu, G.; Yates Jr, J. T. *Chem. Rev.* **1995**, *95*, 735-758.
[19]. Wang, H.; Zhang, L.; Chen, Z.; Hu, J.; S.; Li, Z.; Wang, J. Liu; Wang, X. *Chem. Soc. Rev.* **2014**, *43*, 5234-5244.
[20]. Magalhaes, P.; Andrade, L.; Nunes, O. C.; Mendes, A. *Rev. Adv. Mater. Sci.* **2017**, *51*, 91-129.
[21]. Zhang, J.; Wang, Y.; Jin, J.; Zhang, J.; Lin, Z.; Huang, F.; Yu, *ACS Appl. Mater. Interfaces* **2013**, *5*, 10317-10324.
[22]. Hosseinpour-Mashkani, S. M.; Maddahfar, M.; Sobhani-Nasab, A. *J. Mater. Sci. Mater. Electron.* **2016**, *27*, 474-480.
[23]. Ma, D.; Shi, J. W.; Zou, Y.; Fan, Z.; Ji, X.; Niu C. *ACS appl. Mater. Interfaces* **2017**, *9*, 25377-25386.
[24]. Ikram S. *Arch. Med.* **2016**, *2*, 1-10.
[25]. Maeda, K.; Domen, K. *J. Phys. Chem. Lett.* **2010**, *1*, 2655-2661.
[26]. Elaziouti, A.; Laouedj, N.; Bekka, A.; Vannier, R. N. *J. King Saud. Univ. Sci.* **2015**, *27*, 120-135.
[27]. Beranek, R. *Adv. Phys. Chem.* **2011**, *2011*, 1-20.
[28]. Wang, Y.; Zhang, R.; Li, J.; Li, L.; Lin, S. *Nanoscale Res. Lett.* **2014**, *9*, 46, 1-8.
[29]. Huang, H.; Wang, S.; Zhang, Y.; Chu, P. K. *Rsc Adv.* **2014**, *4*, 41219-41227.
[30]. Xu, Y.; Schoonen, M. A. Am. *Mineral.* **2000**, *85*, 543-556.
[31]. Li, L.; Liu, X.; Zhang, Y.; N. T.; Nuhfer, K.; Barmak, Salvador, P. A.; Rohrer, G. S. *ACS Appl. Mater. Interfaces* **2013**, *5*, 5064-5071.
[32]. Liu, S.; Chen, J.; Xu, D.; Zhang, X.; Shen, M. *J. Mater. Res.* **2018**, *33*, 1391-1400.
[33]. Chen, F.; Yang, Q.; Li, X.; Zeng, G.; Wang, D.; Niu, C.; Zhao, J.; An, H.; Xie, T.; Deng, Y. *Appl. Catal. B. Environ.* **2017**, *200*, 330-342.
[34]. Khanchandani, S.; Kundu, S.; Patra, A.; Ganguli, A. K. *J. Phys. Chem. C* **2013**, *117*, 5558-5567.
[35]. Marschall, R. *Adv. Funct. Mater.* **2014**, *24*, 2421-2440.
[36]. Jang, J. S.; Ahn, C. W.; Won, S. S.; Kim, J. H.; Choi, W.; Lee, B. S.; Yoon, J. H.; Kim, H. G.; Lee, J. S. *J. Phys. Chem. C* **2017**, *121*, 15063-15070.
[37]. Zhang, Z.; Lin, S.; Li, X.; Li, H.; Zhang, T.; Cui, W. *Nanomaterials* **2018**, *8*, 330.
[38]. Ran, J.; Ma, T. Y.; Gao, G.; Du, X. W.; Qiao, S. Z. *Energy Environ. Sci.* **2015**, *8*, 3708-3717.
[39]. Guo, L.; Yang, Z.; Marcus, K.; Li, Z. , Luo, B.; Zhou, L.; Wang, X.; Du, Y.; Yang, Y. *Energy Environ. Sci.* **2018**, *11*, 106-114.
[40]. Qiu, B.; Zhu, Q.; Du, M.; Fan, L.; M.; Xing, Z. *J. Angew. Chem.* **2017**, *129*, 2728-2732.
[41]. Zhang, Z.; Jiang, D.; Li, D.; M.; He, Chen, M. *Appl. Catal. B: Environ.* **2016**, *183*, 113-123.
[42]. Zou, Y.; Shi, J. W.; Ma, D.; Fan, Z.; L.; Cheng, Sun, D.; Wang, Z.; Niu, C. *Chem. Sus. Chem.* **2018**, *11*, 1187-1197.
[43]. Ola, O.; Maroto-Valer, M. M. *J. Photochem. Photobiol. C* **2015**, *24*, 16-42.
[44]. Huang, F.; Yan, A.; Zhao, H. Influences of doping on photocatalytic properties of TiO2 photocatalyst, in: Semiconductor Photocatalysis-Materials, Mechanisms and Applications, InTech, 2016.
[45]. Wang, M.; Ye, M.; Iocozzia, J.; Lin, C.; Lin, Z. *Adv. Sci.* **2016**, *3*, 1600024.
[46]. Tatsuma, T.; Nishi, H.; Ishida, T. *Chem. Sci.* **2017**, *8*, 3325-3337.
[47]. Islam, S. Z.; Nagpure, S.; Kim, D. Y.; Rankin, S. E. *Inorganics* **2017**, *5*, 15.
[48]. Teka, T. *Int. J. Technol. Enhanc. Emerg. Eng. Res.* **2015**, *3*, 2347-4289.
[49]. Yu, W.; Zhang, J.; Peng, T. *Appl. Catal. B: Environ.* **2016**, *181*, 220-227.
[50]. Serpone, N. *J. Phys. Chem. B* **2006**, *110*, 24287-24293.
[51]. Park, H.; Park, Y.; Kim, W.; Choi, W. *J. Photochem. Photobiol. C* **2013**, *15*, 1-20.
[52]. Dai, K.; Peng, T.; Ke, D.; Wei, B. *Nanotechnology* **2009**, *20*, 125603.
[53]. Rawal, S. B.; Bera, S.; Lee, D.; Jang, D. J.; Lee, W. I. *Catal. Sci. Technol.* **2013**, *3*, 1822-1830.
[54]. Baransi, K.; Dubowski, Y.; Sabbah, I. *Water Res.* **2012**, *46*, 789-798.
[55]. Bouazza, N.; Ouzzine, M.; Lillo-Rodenas, M.; Eder, Linares-Solano, D.; A. *Appl. Catal. B: Environ.* **2009**, *92*, 377-383.
[56]. Jiang, D.; Irfan, R. M.; Sun, Z.; Lu, D.; Du, P. *Chem. Sus. Chem.* **2016**, *9*, 3084-3092.
[57]. Moniz, S. J.; Shevlin, S. A.; Martin, D. J.; Guo, Z. X.; Tang, *J. Energy Environ. Sci.* **2015**, *8*, 731-759.
[58]. Paul, K.; Giri, P. Plasmonic Metal and Semiconductor Nanoparticle Decorated TiO2 -Based Photocatalysts for Solar Light Driven Photocatalysis, in: Reference Module in Chemistry, Molecular Sciences and Chemical Engineering, 2017.
[59]. Qi, K.; Cheng, B.; Yu, J.; Ho, W. *Chinese J. Catal.* **2017**, *38*, 1936-1955.
[60]. Li, H.; Tu, W.; Zhou, Y.; Zou, Z. *Adv. Sci.* **2016**, *3*, 1500389.
[61]. Jiang, L.; Yuan, X.; Zeng, G.; Liang, J.; Wu, Z.; Wang, H. *Environ. Sci. Nano* **2018**, *5*, 599-615.
[62]. Xu, Z.; Kibria, M. G.; AlOtaibi, B.; Duchesne, P. N.; Besteiro, L. V.; Gao, Y.; Zhang, Q.; Mi, Z.; Zhang, P.; Govorov, A. O.; Mai, L.; Chaker, M.; Ma, D. *Appl. Catal. B: Environ.* **2018**, *221*, 77-85.
[63]. Lou, Z.; Zhu, M.; Yang, X.; Zhang, Y.; M. -H. *Appl. Catal. B: Environ.* **2018**, *226*, 10-15.
[64]. Fan, W.; Leung, M. K. H. *Molecules* **2016**, *21*, 180.
[65]. Nguyen, B. H.; Nguyen, V. H. *Adv. Nat. Sci-Nanosci.* **2015**, *6*, 043001.
[66]. Xie, L.; Ai, Z.; Zhang, M.; Sun, R.; Zhao, W. *PloS One* **2016**, *11*, e0161397.
[67]. Khan, M. R.; Chuan, T. W.; Yousuf, A.; Chowdhury, M.; Cheng, C. K. *Catal. Sci. Technol.* **2015**, *5*, 2522-2531.
[68]. Erwin, W. R.; Zarick, H. F.; Talbert, E. M.; Bardhan, R. *Energy Environ. Sci.* **2016**, *9*, 1577-1601.
[69]. Colmenares, J. C.; . Luque, R; Campelo, J. M.; Colmenares, F.; Karpinski, Z.; Romero, A. A. *Materials* **2009**, *2*, 2228-2258.
[70]. Buzea, C.; Pacheco, I. I.; Robbie, K. *Biointerphases* **2007**, *2*, MR17-MR71.
[71]. Lin, H.; Huang, C.; Li, W.; Ni, C.; Shah, S. I.; Tseng, Y. -H. *Appl. Catal. B: Environ.* **2006**, *68,* 1-11.
[72]. Bera, D.; Qian, L.; Tseng, T. -K.; Holloway, P. H. *Materials*, **2010**, *3*, 2260-2345.
[73]. Rajabi, H. R.; Karimi, F.; Kazemdehdashti, H.; Kavoshi, L. *J. Photochem. Photobiol. B, Biol.* **2018**, *181*, 98-105.
[74]. Kundu, S.; Patra, A. *Chem. Rev.* **2016**, *117*, 712-757.
[75]. Sarkar, S.; Sardar, S.; Makhal, A.; Dutta, J.; Pal, S. K. Engineering FRET-based solar cells: manipulation of energy and electron transfer processes in a light harvesting assembly, in: High-Efficiency Solar Cells, Springer, 2014.
[76]. Wu, P.; Yan, X. P. *Chem. Soc. Rev.* **2013**, *42*, 5489-5521.
[77]. Li, J.; Cushing, S. K.; Meng, F.; Senty, T. R.; Bristow, A. D.; Wu, N. *Nat. Photonics*, **2015**, *9(9)*, 601-607.
[78]. Chen, Y.; Lu, Q.; Yan, X.; Mo, Q.; Chen, Y.; Liu, B.; Teng, L.; Xiao, W.; Ge, L.; Wang, Q. *Nanoscale Res. Lett.* **2016**, *11*, 60.